

# A Fortran 90 Hartree-Fock program for one-dimensional periodic $\pi$ -conjugated systems using Pariser-Parr-Pople model

Kodayya Gundra<sup>1</sup>, Alok Shukla

*Department of Physics, Indian Institute of Technology, Bombay, Powai, Mumbai 400076, INDIA*

---

## Abstract

Pariser-Parr-Pople (P-P-P) model Hamiltonian is employed frequently to study the electronic structure and optical properties of  $\pi$ -conjugated systems. In this paper we describe a Fortran 90 computer program which uses the P-P-P model Hamiltonian to solve the Hartree-Fock (HF) equation for infinitely long, one-dimensional, periodic,  $\pi$ -electron systems. The code is capable of computing the band structure, as also the linear optical absorption spectrum, by using the tight-binding (TB) and the HF methods. Furthermore, using our program the user can solve the HF equation in the presence of a finite external electric field, thereby, allowing the simulation of gated systems. We apply our code to compute various properties of polymers such as *trans*-polyacetylene (*t*-PA), poly-*para*-phenylene (PPP), and armchair and zigzag graphene nanoribbons, in the infinite length limit.

*Keywords:* Hartree-Fock method, self-consistent field approach

P-P-P model Hamiltonian, Periodic boundary conditions

*PACS:* 31.15.xr, 31.15.Ne, 31.15.bu, 31.15.-p

---

## Program Summary

*Title of program:* ppp\_bulk.x

*Catalogue Identifier:*

*Program summary URL:* E\_F

*Program obtainable from:* CPC Program Library, Queen's University of Belfast, N. Ireland

*Distribution format:* tar.gz

*Computers :* PC's/Linux

*Linux Distribution:* Code was developed and tested on various recent versions

---

*Email addresses:* [naiduk@barc.gov.in](mailto:naiduk@barc.gov.in) (Kodayya Gundra), [shukla@phy.iitb.ac.in](mailto:shukla@phy.iitb.ac.in) (Alok Shukla)

<sup>1</sup>Permanent address: Theoretical Physics Division, Bhabha Atomic Research Centre, Mumbai 400085, INDIA

of 64-bit Fedora including Fedora 14 (kernel version 2.6.35.12-90)

*Programming language used:* Fortran 90

*Compilers used:* Program has been tested with Intel Fortran Compiler (non-commercial version 11.0.074) and gfortran compiler (gcc version 4.5.1) with optimization option -O.

*Libraries needed:* This program needs to link with LAPACK/BLAS libraries compiled with the same compiler as the program. For the Intel Fortran Compiler we used the ACML library version 4.4.0, while for the gfortran compiler we used the libraries supplied with the Fedora distribution.

*Number of bytes in distributed program, including test data, etc.:* ... size of the tar file

*Number of lines in distributed program, including test data, etc.:* ... lines in the tar file

*Card punching code:* ASCII

*Nature of physical problem:* The electronic structure of one-dimensional periodic  $\pi$ -conjugated systems is an intense area of research at present because of the tremendous interest in the physics of conjugated polymers and graphene nanoribbons. The computer program described in this paper provides an efficient way of solving the Hartree-Fock equations for such systems within the P-P-P model. In addition to the Bloch orbitals, band structure, and the density of states, the program can also compute quantities such as the linear absorption spectrum, and the electro-absorption spectrum of these systems.

*Method of Solution:* For a one-dimensional periodic  $\pi$ -conjugated system lying in the  $xy$ -plane, the single-particle Bloch orbitals are expressed as linear combinations of  $p_z$ -orbitals of individual atoms. Then using various parameters defining the P-P-P Hamiltonian, the Hartree-Fock equations are set up as a matrix eigenvalue problem in the  $k$ -space. Thereby, its solutions are obtained in a self-consistent manner, using the iterative diagonalizing technique at several  $k$ -points. The band structure and the corresponding Bloch orbitals thus obtained are used to perform a variety of calculations such as the density of states, linear optical absorption spectrum, electro-absorption spectrum, *etc.*

*Running Time:* Most of the examples provided take only a few seconds to run. For a large system, however, depending on the system size, the run time may be a few minutes to a few hours.

*Unusual features of the program:* None

## 1. Introduction

Conjugated molecules and polymers have been actively investigated theoretically as well as experimentally in recent years, (author?) [1, 2, 3] because of their potential applications in manufacture of optoelectronic devices, and solar cells (author?) [4]. The low-lying excitations in such materials are characterized by the  $\pi$  electrons, which have itinerant nature, and form the energy levels near the chemical potential (Fermi level). Recently, the field of  $\pi$ -conjugated systems has received a tremendous boost with the synthesis of graphene (author?) [5],

and its heterostructures such as graphene nanoribbons (author?) [6], which exhibit exotic transport and electronic properties, leading to the possibility of future electronic devices based upon graphene rather than silicon (author?) [7, 8, 9]. Because of these recent advances, theoretical studies of  $\pi$ -electron systems have come to the forefront of physics. Most of the theoretical methods used for describing the electronic structure of these materials can be classified as: (a) fully *ab initio* approaches based upon the mean-field methods such as the density-functional theory (DFT) (author?) [10, 11, 12, 13, 14, 15] or the Hartree-Fock (HF) method (author?) [16, 17, 18, 19], and (b) approaches based upon effective  $\pi$ -electron models such as the tight-binding (TB) model (author?) [20, 21, 22], and the Hubbard (author?) [23, 24, 25] or the extended Hubbard model (author?) [26]. The *ab initio* methods are generally computationally intensive because they make no distinction between the  $\sigma$  and the  $\pi$  electrons of the system, and therefore require the use of large basis sets to provide a reasonable description of the electronic structure of such systems. In case of graphene nanoribbons (GNRs) of large widths, and also polymers with large unit cells, the number of degrees of freedom involved in the problem may impose severe limitations on the problems which can be solved computationally. On the other hand the main advantage of the effective  $\pi$ -electron model Hamiltonians is that they explicitly deal only with the  $\pi$  electrons, thereby reducing the degrees of freedom considerably, and, thus allowing the simulation of much larger systems as compared to the *ab initio* approaches. Their disadvantage, of course, is that they are semiempirical in nature, and, therefore, the parameters involved in them are often determined using the spectroscopic data of a suitable model system. Nevertheless, when calculations on very large systems need to be performed, often it is virtually impossible to use the *ab initio* approaches, and, therefore, model Hamiltonians provide an attractive alternative. Even for smaller systems, model Hamiltonians allow us to understand the underlying physics in simple terms, therefore, aforesaid  $\pi$ -electron approaches are very popular when it comes to calculations of the electronic structure of graphene and its nanostructures.

Among the effective  $\pi$ -electron approaches, the TB model (called the Hückel model in the chemistry literature) is the simplest, but it does not incorporate the effect of electron-electron (e-e) repulsion. The Hubbard model and its extended versions go beyond the TB approach, and incorporate the short-range parts of the Coulomb repulsion such as the on-site, and the nearest-neighbor interactions, respectively. In chemistry literature it is well-known that in  $\pi$ -electron systems such as various aromatic molecules and conjugated polymers, the role of long-range e-e interactions cannot be ignored when it comes to their electronic structure (author?) [1, 2, 3]. And, indeed, Pariser-Parr-Pople (P-P-P) model Hamiltonian (author?) [27], which is an effective  $\pi$ -electron Hamiltonian incorporating long-range e-e interaction, has been used with considerable success in describing the physics of such systems (author?) [1, 2, 3]. Thus, it is logical to conclude that such e-e interactions will also be important in understanding the physics of the graphene-based materials. In recent years, our group and collaborators (author?) [28, 29, 30, 31, 32, 33, 34, 35, 36, 37, 38, 39, 40],

along with numerous other groups(**author?**) [1, 2, 3, 41, 42, 43, 44, 45, 46], have used the P-P-P model to study the electronic structure and optical properties of conjugated molecules and oligomers. For finite  $\pi$ -conjugated systems, in our group, we have developed a general-purpose HF program employing the P-P-P model, which is available to anyone for scientific work(**author?**) [47]. However, GNRs and some  $\pi$ -conjugated polymers are believed to be quasi-one-dimensional systems, which need to be studied in the infinite-length limit. Thus, in order to study their electronic structure and related properties, using the P-P-P model (or any other Hamiltonian), one needs to impose periodic boundary conditions, and perform infinite lattice sums to account for their infinite extent, which, our earlier computer program(**author?**) [47] lacks. With this aim in mind, we recently developed a P-P-P model-based computer program, which solves both the restricted HF (RHF) and the unrestricted HF (UHF) equations for one-dimensional periodic systems, and used it to study the electronic structure and optical properties of mono-layer and multilayer GNRs of various kinds(**author?**) [48, 49]. The ability to solve the UHF equations allows us to explore magnetic properties of polymers and GNRs. The aim of the present paper is to describe the computer program in detail, and make it available for use by anyone interested in the physics of GNRs and  $\pi$ -conjugated polymers. The program is capable of computing the total energy, the band structure, the density of states (DOS), and also the interband optical absorption spectrum in form of the frequency-dependent dielectric response tensor, both with and without an external homogeneous electric field. The fact that our program can solve the HF equations in the presence of an external electric field allows the user to explore gated configurations of polymers and GNRs. In this work, we demonstrate the capabilities of our program by performing calculations on polymers *trans*-polyacetylene (*t*-PA), poly-*para*-phenylene (PPP), armchair GNRs (AGNRs), and zigzag GNRs (ZGNRs) of various widths. We also note that Nakada *et al.*(**author?**) [50] reported a P-P-P model based band structure calculation of both AGNRs and ZGNRs several years back.

The remainder of the paper is organized as follows. In section 2 we briefly review the theory associated with the P-P-P model Hamiltonian. Next, in section 3 we discuss the general structure of our computer program, and also describe its constituent subroutines. In section 4 we briefly describe how to install the program on a given computer system, and to prepare the input files. Results of various example calculations using our program are presented and discussed in section 5. Finally, in section 6, we present our conclusions, as well as discuss possible future directions.

## 2. Theory

In this section we briefly discuss the theory behind our computer program.

### 2.1. Pariser-Parr-Pople Hamiltonian

The P-P-P model Hamiltonian(**author?**) [27], with one  $\pi$ -electron per carbon atom, is given by

$$H = \sum_{i,\sigma} \epsilon_i c_{i\sigma}^\dagger c_{i\sigma} - \sum_{i,j,\sigma} t_{ij} (c_{i\sigma}^\dagger c_{j\sigma} + c_{j\sigma}^\dagger c_{i\sigma}) + U \sum_i n_{i\uparrow} n_{i\downarrow} + \sum_{i<j} V_{ij} (n_i - 1)(n_j - 1) \quad (1)$$

where  $\epsilon_i$  represents the site energy associated with the  $i$ th carbon atom,  $c_{i\sigma}^\dagger$  creates an electron of spin  $\sigma$  on the  $p_z$  orbital of atom  $i$ ,  $n_{i\sigma} = c_{i\sigma}^\dagger c_{i\sigma}$  is the number of electrons with the spin  $\sigma$ , and  $n_i = \sum_\sigma n_{i\sigma}$  is the total number of electrons on atom  $i$ . The parameters  $U$  and  $V_{ij}$  are the on-site and long-range Coulomb interactions, respectively, while  $t_{ij}$  is the one-electron hopping matrix element. On setting  $V_{ij} = 0$  (with  $U \neq 0$ ), the Hamiltonian reduces to the Hubbard model, while on setting both  $U = 0$  and  $V_{ij} = 0$ , the tight-binding (TB) model is obtained. The parametrization of Coulomb interactions is Ohno like(**author?**) [51],

$$V_{i,j} = \frac{U}{\kappa_{i,j} (1 + 0.6117 R_{i,j}^2)^{1/2}}, \quad (2)$$

where,  $\kappa_{i,j}$  depicts the dielectric constant of the system which can simulate the effects of screening, and  $R_{i,j}$  is the distance in Å between the  $i$ -th and the  $j$ -th carbon atoms. In our earlier work on GNRs(**author?**) [48], we used the *ab-initio* GW band structure of mono layer AGNR-12 (AGNR- $N_A$ , denotes an AGNR with  $N_A$  dimer lines across the width) reported by Son *et al.*(**author?**) [10] to obtain a set of “modified screened Coulomb parameters,” with  $U = 6.0$  eV and  $\kappa_{i,j} = 2.0$  ( $i \neq j$ ) and  $\kappa_{i,i} = 1$ , which are slightly different from the screened parameters reported initially by Chandross and Mazumdar(**author?**) [52], with  $U = 8.0$  eV and  $\kappa_{i,j} = 2.0$  ( $i \neq j$ ) and  $\kappa_{i,i} = 1$ , aimed at describing the optical properties of phenyl-based polymers within the P-P-P model. The modified screened parameters provided good agreement between our HF band gaps, and those obtained by the GW method for a few AGNRs, however, for ZGNRs the agreement was not good(**author?**) [48]. In this work, we examine the issue of the choice of Coulomb parameters in a critical manner, and conclude that no single set of parameters gives uniformly good agreements between our results and the GW results for all types of GNRs. In section 5, where this issue is investigated, we find that a set of parameters which provides excellent agreement between ours and GW results for a class of GNRs, may simply fail to reproduce such agreement for another class of GNRs. In other words, the choice of Coulomb parameters which will lead to good agreement between our HF results, and the *ab initio* GW ones, depends upon the geometries of the GNRs in question. Thus, after trying a number of Coulomb parameters, and in the absence of any experimental data on the band gaps of GNRs, we have decided it is best to use the original screened parameters of Chandross and Mazumdar(**author?**) [52], with  $U = 8.0$  eV and  $\kappa_{i,j} = 2.0$  ( $i \neq j$ ) and  $\kappa_{i,i} = 1$

for all the GNRs. But, we would like to emphasize that the user has the freedom to choose a different set of Coulomb parameters as per the requirements, and, we encourage such experimentation.

## 2.2. Unrestricted Hartree-Fock Equations

We have implemented the RHF and the UHF methods within the P-P-P model, using the standard linear combination of atomic orbitals (LCAO) formalism. We shall review the basics of the formalism for the UHF method (also known as the Pople-Nesbet formalism **(author?)** [53]), from which the corresponding equations for the RHF method can be easily deduced. In this approach, the  $n$ -th Bloch orbital of the system corresponding to the spin up electrons ( $\alpha/\beta$  will denote spin up/down electrons) is expressed as a linear combination of  $m$  basis functions per unit cell,

$$\psi_n^{(\alpha)}(k) = \sum_{\mu=1}^m C_{\mu n}^{(\alpha)}(k) \phi_{\mu}(k) \quad (3)$$

where  $C_{\mu n}^{(\alpha)}(k)$ 's represent the linear expansion coefficients, to be determined at a set of  $k$ -points in the first Brillouin zone (BZ), and the  $\mu$ -th Bloch function  $\phi_{\mu}(k)$  is given by

$$\phi_{\mu}(k) = \frac{1}{\sqrt{N}} \sum_j e^{ikR_j} \phi_{\mu}(r - R_j) \quad (4)$$

where  $N \rightarrow \infty$  is the total number of unit cells in the system,  $\phi_{\mu}(r - R_j)$  is the atomic orbital (AO) ( $p_z$  orbital mentioned in section 2.1) located in the  $j^{th}$  unit cell defined by the lattice vector  $R_j$ . The definition of the Bloch orbital corresponding to the spin down electrons will be identical, with  $\alpha$  replaced by  $\beta$  in Eq. 3. Because, in the P-P-P model, the basis functions  $\phi_{\mu}(r - R_j)$  are assumed to form an orthonormal set, the UHF equation for up-spin orbitals can be written in the matrix form as

$$F^{\alpha}(k) C_n^{\alpha}(k) = \epsilon_n^{\alpha}(k) C_n^{\alpha}(k) \quad (5)$$

where, for a given  $k$  value,  $F^{\alpha}(k)$  represents the Fock matrix for the up-spin electrons,  $C_n^{\alpha}(k)$  represents the corresponding  $C_{\mu n}^{(\alpha)}(k)$  coefficients, arranged in form of a column vector, and  $\epsilon_n^{\alpha}(k)$  denotes the band eigenvalue. The Fock operator for electrons of up spin is given by

$$F^{\alpha}(k) = h(k) + (J^{\alpha}(k) + J^{\beta}(k) - K^{\alpha}(k)) \quad (6)$$

where  $h(k)$  denotes the Fourier transform of the one-electron parts of the P-P-P Hamiltonian (*cf.* Eq. 1),  $J^{\alpha}(k)/K^{\alpha}(k)$  are the Coulomb/exchange integrals for the up spin electrons, obtained by Fourier transforming their real-space

counterparts

$$h_{\mu\nu}(k) = \sum_{j=-\infty}^{\infty} e^{ikR_j} h_{\mu\nu}(R_j), \quad (7)$$

$$J_{\mu\nu}^{\alpha}(k) = \sum_{j=-\infty}^{\infty} e^{ikR_j} J_{\mu\nu}^{\alpha}(R_j), \quad (8)$$

$$K_{\mu\nu}^{\alpha}(k) = \sum_{j=-\infty}^{\infty} e^{ikR_j} K_{\mu\nu}^{\alpha}(R_j). \quad (9)$$

Above  $h_{\mu\nu}(R_j)$  is the one-electron part of the P-P-P Hamiltonian, and  $J_{\mu\nu}^{\alpha}(R_j)/K_{\mu\nu}^{\alpha}(R_j)$  denote the Coulomb/exchange integrals in the real space, defined as

$$J_{\mu\nu}^{\alpha}(R_j) = \sum_{\sigma=1}^m \sum_{\lambda=1}^m \sum_{k=-\infty}^{\infty} D_{\sigma\lambda}^{\alpha}(R_k) \sum_{l=-\infty}^{\infty} \langle \mu(o)\sigma(R_l) | \frac{1}{r_{12}} | \nu(R_j)\lambda(R_l + R_k) \rangle, \quad (10)$$

and

$$K_{\mu\nu}^{\alpha}(R_j) = \sum_{\sigma=1}^m \sum_{\lambda=1}^m \sum_{k=-\infty}^{\infty} D_{\sigma\lambda}^{\alpha}(R_k) \sum_{l=-\infty}^{\infty} \langle \mu(o)\sigma(R_l) | \frac{1}{r_{12}} | \lambda(R_l + R_k)\nu(R_j) \rangle, \quad (11)$$

where the expression for a general two-electron repulsion integrals is

$$\begin{aligned} \langle \mu(R_i)\sigma(R_j) | \frac{1}{r_{12}} | \nu(R_k)\lambda(R_l) \rangle &= \int \int \phi_{\mu}(\mathbf{r}_1 - R_i) \phi_{\nu}(\mathbf{r}_1 - R_k) r_{12}^{-1} \\ &\times \phi_{\sigma}(\mathbf{r}_2 - R_j) \phi_{\lambda}(\mathbf{r}_2 - R_l) d^3\mathbf{r}_1 d^3\mathbf{r}_2, \end{aligned} \quad (12)$$

and the density matrix for the up-spin electrons,  $D_{\mu\nu}^{\alpha}(R_j)$ , is given by

$$D_{\mu\nu}^{\alpha}(R_j) = \frac{1}{\Delta} \int \sum_{n=1}^{n_{\alpha}} C_{\mu n}^{\alpha*}(k) C_{\nu n}^{\alpha}(k) e^{ikR_j} dk, \quad (13)$$

where the integral over  $k$  is performed over the one-dimensional (1D) BZ of length  $\Delta$ , and  $n_{\alpha}$  denotes the number of up-spin electrons per unit cell. Above we have given the explicit expressions of various quantities for their up-spin components only, because the expressions for the down-spin components can be obtained simply by interchanging  $\alpha$  and  $\beta$ . The total energy per unit cell of a given system is computed using the real-space expression

$$\begin{aligned} E_{\text{cell}} &= \sum_j \sum_{\mu,\nu} \{ D_{\mu\nu}^{\alpha}(R_j) h_{\mu\nu}(R_j) + \frac{1}{2} D_{\mu\nu}^{\alpha}(R_j) (J_{\mu\nu}^{\alpha}(R_j) - K_{\mu\nu}^{\alpha}(R_j)) \\ &+ \frac{1}{2} D_{\mu\nu}^{\beta}(R_j) (J_{\mu\nu}^{\beta}(R_j) - K_{\mu\nu}^{\beta}(R_j)) + D_{\mu\nu}^{\beta}(R_j) J_{\mu\nu}^{\alpha}(R_j) \}, \end{aligned} \quad (14)$$

where  $D_{\mu\nu}(R_j) = D_{\mu\nu}^\alpha(R_j) + D_{\mu\nu}^\beta(R_j)$ , denotes the total density matrix of the system. The expressions of the two-electron integrals appearing in Eqs. 10 and 11 are of the most general type, however, in case of the P-P-P model (*cf.* Eq. 1) only density-density type of e-e repulsion terms are included, which implies

$$\langle \mu(R_i)\sigma(R_j) | \frac{1}{r_{12}} | \nu(R_k)\lambda(R_l) \rangle = \delta_{\mu\nu}\delta_{\sigma\lambda}\delta_{R_i R_k}\delta_{R_j R_l} V_{\mu(o)\lambda(R_j-R_i)} \quad (15)$$

where  $V_{\mu(o)\lambda(R_j-R_i)}$  implies that expression is calculated using Eq. 2, assuming that the  $\mu$ -th basis function is located in the reference unit cell while the  $\lambda$ -th basis function is in the cell with location  $R_j - R_i$ . After the simplification of Eq. 15, evaluation of  $J_{\mu\nu}^\alpha(R_j)$  and  $K_{\mu\nu}^\alpha(R_j)$  becomes quite easy: (a) in Eq. 10 only an infinite lattice sum over  $R_l$  needs to be performed, which is done by including a large number of terms, and (b) in Eq. 11 both the sums for  $R_k$  and  $R_l$  reduce to one term each. The convergence of our calculations with respect to these lattice sums was tested extensively.

The UHF equations of the system, leading to the band structure  $(\epsilon_n^{(\alpha)}(k)/\epsilon_n^{(\beta)}(k))$ , and the corresponding Bloch orbitals, are obtained by solving Eq.5, and its  $\beta$ -spin counterpart, by iterative diagonalization technique at a set of  $k$ -points, until the total energy per cell of the system (*cf.* Eq. 14) converges. During the self-consistent HF iterations, the integration over the BZ is performed using the Gauss-Legendre quadrature technique as suggested by André *et al.* (author?) [54], with the additional flexibility that the number of points used for the quadrature can be chosen by the user.

In order to perform calculations in the presence of a static external electric field to simulate the gate bias, one can solve the HF equations using a modified Fock operator under the electric dipole approximation by introducing the corresponding term containing the uniform electric field  $\mathbf{E}$ . The modified Fock operator of the system is then given by

$$F_{efield}^\alpha = F^\alpha - \boldsymbol{\mu} \cdot \mathbf{E} = F^\alpha + |e|\mathbf{E} \cdot \mathbf{r}, \quad (16)$$

where  $F^\alpha$  is the unperturbed Fock operator for the up-spin electrons in the absence of the electric field,  $e$  represents the electronic charge,  $\boldsymbol{\mu} = -e\mathbf{r}$ , is the dipole operator, and  $\mathbf{r}$  is the position operator for which the usual diagonal representation is employed.

### 2.3. Density of states

The density of states (DOS) is obtained using the well-known expression

$$\rho(\epsilon) = C \sum_i \int e^{-(\epsilon - \epsilon_i(k))^2 / 2\gamma^2} dk \quad (17)$$

where  $\epsilon$  is energy at which DOS is computed,  $\epsilon_i(k)$  is the energy of  $i$ -th orbital at a given  $k$  point,  $\gamma$  is the broadening parameter, and  $C$  includes the rest of the



constants. The integration over  $k$  is performed over the 1D BZ, and summation over  $i$  includes all the Bloch orbitals of the system. In our calculations we set  $C = 1$  to obtain the DOS in the arbitrary units.

#### 2.4. Theory of optical absorption

The optical absorption spectrum of the incident radiation polarized in  $x$  or  $y$  direction is computed in the form of the corresponding components of the imaginary part of the dielectric constant tensor, i.e.,  $\epsilon_{ii}(\omega)$ , using the standard formula

$$\epsilon_{ii}(\omega) = C \sum_{v,c} \int \frac{|\langle c(k)|p_i|v(k)\rangle|^2}{\{(E_{cv}(k) - \hbar\omega)^2 + \gamma^2\}E_{cv}^2(k)} dk, \quad (18)$$

where  $p_i$  denotes the momentum operator in the  $i$ -th Cartesian direction,  $\omega$  represents the angular frequency of the incident radiation,  $E_{cv}(k) = \epsilon_c(k) - \epsilon_v(k)$ , with  $\epsilon_c(k)$  ( $\epsilon_v(k)$ ) being the conduction band (valence band) eigenvalues of the Fock matrix,  $\gamma$  is the line width, while  $C$  includes rest of the constants. Assuming that the valence band eigen state  $|v(k)\rangle$  is expressed as (*cf.* Eq. 3, ignoring the spin orientation)

$$|v(k)\rangle = \sum_{\mu} C_{\mu v}(k) |\chi_{\mu}(k)\rangle,$$

with a similar expression for the conduction band eigen states  $|c(k)\rangle$ . The momentum matrix elements  $\langle c(k)|p_i|v(k)\rangle$  needed to compute  $\epsilon_{ii}(\omega)$ , for a 1D periodic system, can be calculated using the formula, **(author?)** [55]

$$\begin{aligned} \langle c(k)|p_i|v(k)\rangle &= \delta_{i,1} \frac{m_0}{\hbar} \sum_{\mu,\nu} C_{\nu c}^*(k) C_{\mu v}(k) \frac{\partial}{\partial k} H_{\nu\mu}(k) \\ &+ \frac{im_0(\epsilon_c(k) - \epsilon_v(k))}{\hbar} \sum_{\mu,\nu} C_{\nu c}^*(k) C_{\mu v}(k) d_{\mu\nu}^{(i)}, \end{aligned} \quad (19)$$

where  $\delta_{i,1}$  implies that the term is nonzero when  $i$  denotes the periodicity direction ( $x$  direction),  $m_0$  is the free-electron mass,  $\frac{\partial}{\partial k} H_{\nu\mu}(k)$  represents the derivative of the Hamiltonian (Fock matrix, in the present case) with respect to  $k$ ,  $d_{\mu\nu}^{(i)}$  denotes the matrix elements of the  $i$ -th component of the position operator  $\mathbf{d}$  defined with respect to the reference unit cell, and accounts for the so-called intra-atomic contribution **(author?)** [55]. Note that Eq. 19 can also be used to compute the matrix element  $\langle c(k)|p_y|v(k)\rangle$  needed to calculate the absorption spectrum for the  $y$ -polarized light for GNRs (which are periodic only in the  $x$  direction), by setting the first term on its right hand side to zero, and retaining the contribution only of the second term. In these calculations,  $\frac{\partial}{\partial k} H_{\nu\mu}(k)$  was computed numerically, while the usual diagonal representation was employed for the  $\mathbf{d}$  operator. Furthermore, we set  $C = 1$  in all the cases to obtain the absorption spectra in arbitrary units.

### 3. Description of the Program

Theoretical formalism described in the preceding section has been implemented numerically in a computer program called “ppp\_bulk.x” using the Fortran 90 (F90) programming language. Advanced features of F90, such as the dynamic memory allocation, modules, etc., have been used to improve the efficiency of the code. Architecture independent numerical precision is used for portability of the code across different computer architectures. This program is capable of doing both the tight binding as well as P-P-P model calculations. Using a small number of input parameters such as the positions of the atoms in the unit cell, lattice translation vector, hopping and P-P-P Coulomb parameters etc., ppp\_bulk.x determines the band structure, density of states, joint density of states, optical and electro absorption spectrum for 1D periodic  $\pi$ -conjugated systems. As mentioned earlier, the lattice sums are performed in real space by including a large number of unit cells, and integration along the BZ was performed using the Gauss-Legendre quadrature approach (author?) [54]. The convergence of SCF iterations is slow for systems with large number of electrons, therefore, we have also implemented the method of damping to speed up the convergence.

Our computer code consists of the main program, and various subroutines. Optionally, the user can link to the LAPACK/BLAS libraries, whose diagonalization routines can be used by our program. In the following we briefly describe the main program, as well as each subroutine/function.

#### 3.1. Module *MTYPES*

In this module the precision of REAL variables used throughout the program is defined. This will facilitate machine independent precision for REAL variables.

#### 3.2. Module *MCOMMONDATA*

Global data shared by several routines in the program is defined in this module.

#### 3.3. Main program *PPP\_BULK*

This is the main program of our package for performing electronic structure calculations within a semiempirical TB formalism for 1D periodic systems. It calls other subroutines to accomplish various tasks.

#### 3.4. Subroutine *INPUT*

This routine reads input data such as which Hamiltonian to use, its parametrization, total number of atoms in the unit cell, their Cartesian coordinates, 1D lattice constant, and number of  $k$ -points ( $n_k$ ) for BZ sampling etc. Besides, this subprogram reads the options to perform various types of calculations such as tight binding, RHF, UHF etc. This subroutine also reads the components of external electric field in the units of V/Å, if calculations for a gated configuration

need to be performed. Alternatively, by calling other routines, one can generate coordinates of some important structural units such as AGNRs and ZGNRs of different widths to facilitate an easy realization of the GNR under consideration. In addition, various arrays are allocated dynamically and deallocated after the desired task is completed.

### 3.5. Subroutine *GNR\_RATOM*

This routine generates the coordinates of various atoms in the unit cell of the given GNR, based upon the user specified data consisting of the type of GNR (AGNR or ZGNR), its width, and the nearest-neighbor bond length. It also computes the lattice translation vector.

### 3.6. Subroutine *ERROR*

This routine writes out a fatal error message to a user specified logical unit, and stops the execution of the code.

### 3.7. Subroutine *SORT*

This routine, adapted from Ref. **(author?)** [56], generates an array in which distances between different pairs of atoms in the system are stored in the ascending order.

### 3.8. Subroutine *GET\_NN*

This routine uses the array generated by subroutine SORT to compute the distance between pair of atoms which are nearest neighbors (NN), second NN, third NN and so on depending on the number of unique hoppings defined.

### 3.9. Subroutine *get\_NTij*

This subroutine computes the total number of hopping matrix elements connecting various atomic sites in the system.

### 3.10. Subroutine *HOPPING*

This routine generates the hopping matrix elements connecting various sites. Hopping matrix elements are assigned for a pair of atoms depending on the distance between them. The unique hopping matrix elements are defined by user in the input file starting from NN atoms, followed by the second NN atoms, and so on.

### 3.11. Subroutine *IJPK*

This subroutine is used to pack the row index  $i$  and column index  $j$  of an element of the upper triangle of a real symmetric matrix into an integer corresponding to its location in a 1D array.

### 3.12. Subroutine *INVIJPK*

The task of this subroutine is just the reverse of the subroutine *IJPK*, *i.e.*, it is used to unpack the integers  $i$  (row index) and  $j$  (column index) from the location of the corresponding matrix element of an upper-triangular symmetric matrix packed in a 1D array.

### 3.13. Subroutine *CHEKEDGE*

This subroutine is used to find whether a given site lies on the edge or in the interior of the system. It calculates the  $NN$  for the given site, and if  $NN = 2$  then it is regarded as an edge site, and if  $NN = 3$  then it is a site in the interior of the system.

### 3.14. Subroutine *FILOPN*

This subroutine is meant for opening a file which may either be new or old.

### 3.15. Subroutine *FILCLS*

This subroutine is meant for closing an already open file.

### 3.16. Function *DOTPD*

This function calculates the dot product between two given vectors.

### 3.17. Subroutine *GETNA*

Assuming that a given lattice vector ( $\mathbf{r}$ ) is in the form  $\mathbf{r} = n\mathbf{a}$  and finds the integer  $n$ , where  $\mathbf{a}$  is the primitive vector of the lattice.

### 3.18. Subroutine *PPP\_PARA*

This subroutine generates parameters associated with the P-P-P Hamiltonian, as per the user choice.

### 3.19. Subroutine *PRINTR*

This subroutine prints the coordinates of the unit cell in an output file called 'unitcell.xsf', which can be viewed using the visualization packages such as *xcrysden*(**author?**) [57]. Additionally it also generates an output file called 'system.xsf' in which coordinates of atoms in several unit cells are printed for viewing the periodic system under consideration.

### 3.20. Subroutine *CELL\_DRV*

This is the driver routine for generating the unit cell related data by calling another subroutine named 'cell\_1d'.

### 3.21. Subroutine *CELL\_1D*

Starting with the primitive cell and the lattice vector related data, it generates the coordinates of all the cells and atoms included in the calculations. This data is useful when lattice sums, to account for the long-range Coulomb interactions, are performed.

### 3.22. Subroutine *MATEL\_R*

This is the master routine meant for generating the one- and two-electron matrix elements in the real space, with, or without, the external electric field. This is done based upon the data specified by the user in the input file such as the Hamiltonian under consideration, Coulomb parameters to be used (if any), hopping matrix elements connecting various sites, *etc.*

### 3.23. Subroutine *READ\_Ri*

This routine reads the coordinates of atoms in different unit cells, generated by the routine *cell\_1d*, for performing real space lattice sums.

### 3.24. Subroutine *Makntpq*

This routine arranges the unit cells in an order required for performing real-space lattice sums. The reference unit cell is numbered '0', the unit cells to the right of reference unit cells are identified labeled with positive integers, and the unit cells to its left are labeled with negative integers.

### 3.25. Subroutine *Maktmat*

This routine stores the hopping matrix elements in a translationally invariant format. In this format each hopping element is stored as  $t_{ij}(ipq)$ , where orbital  $i$  is assumed to be in the cell at location  $ipq$ , while orbital  $j$  is in the reference cell.

### 3.26. Subroutine *NUCNUC*

This subroutine computes real space nucleus-nucleus repulsion term for the P-P-P model.

### 3.27. Subroutine *ELE\_NUC*

This subroutine computes real space electron-nucleus repulsion term for the P-P-P model.

### 3.28. Subroutine *COULOMB*

This subroutine computes the long-range Coulomb part of the e-e repulsion term  $J_{\mu\nu}(R_j)$  (*cf.* Eq. 10) for the P-P-P model.

### 3.29. Subroutine *EXCHANGE*

This subroutine computes the long-range exchange part of the e-e repulsion term  $K_{\mu\nu}(R_j)$  (*cf.* Eq. 11) corresponding to the P-P-P Hamiltonian.

### 3.30. Subroutine *gen\_Kmesh*

This subroutine creates  $k$ -points in the positive part of the first BZ of a 1D system, between the limits 0 and  $\pi$ . Various  $k$ -points are non-equidistant, and chosen in accordance with the Gauss-Legendre quadrature. The BZ integration is performed for the dimensionless variable  $ka$ ,  $a$  being the lattice constant.

### 3.31. Subroutine GAULEG

This subroutine generates the roots and weights needed for the Gauss-Legendre quadrature meant for BZ integration.

### 3.32. Subroutine SCF\_DRV

This is the driver routine for carrying out the iterative self-consistent field (SCF) calculations.

### 3.33. Module MSCF\_VAR

This module defines the variables common to routines that perform SCF iterations. In addition, subroutines for allocation and deallocation of several arrays are also defined in this module.

### 3.34. Subroutine SCF\_RHF

This subroutine solves the RHF equations for the system under consideration in a self-consistent manner, using the iterative diagonalization procedure at each  $k$ -point, and returns the canonical SCF orbitals, their eigenvalues, and the total energy per unit cell of the system. The arrays which are needed during the calculations are allocated before the calculations begins, and are deallocated upon its completion. Before the first iteration, Hückel model Hamiltonian is diagonalized to obtain a set of starting orbitals. Subsequently, the Fock matrix corresponding to those orbitals is constructed, and diagonalized. The process is repeated until the self-consistency is achieved. Depending upon the choice of the user, the eigenvalues and eigen vectors can be obtained using either the ZHPEV subroutine from the LAPACK/BLAS library, or the inbuilt HOUSEH\_C subroutine(**author?**) [58], based upon the Householder diagonalization scheme.

### 3.35. Subroutine SCF\_UHF

This subroutine is exactly the same in its logic and structure as the previously described SCF\_RHF, except that the task of this routine is to solve the UHF equation for the system under consideration. Different Fock matrices for the  $\alpha$  and the  $\beta$  spin are constructed and diagonalized in each iteration, until the self-consistency is achieved. Eigenvalues and eigen vectors are computed using the routine ZHPEV/HOUSEH\_C. The iterations are stopped once the total UHF energy of the system converges to within a user defined threshold.

### 3.36. Subroutine COMMUL

This subroutine computes the product of two complex numbers, and returns the real and imaginary parts of the product, separately.

### 3.37. Subroutine GRADFK

This subroutine finds the  $k$ -space derivative of Fock matrix ( $\frac{\partial F(k)}{\partial k}$ ), using the central difference formula. Recall that  $\frac{\partial F(k)}{\partial k}$  is needed to evaluate the momentum matrix elements (*cf.* Eq. 19) required for computing the linear optical absorption spectrum.

### 3.38. Subroutine BAND

This subroutine computes the band structure of the system by diagonalizing the converged Fock matrix at a large number of uniformly-spaced set of  $k$  points. For the purpose, the Fock matrix at those  $k$  points is obtained by Fourier transforming converged Fock matrix in the real space. The Fock matrix in the  $k$ -space is diagonalized using the subroutine ZHPEV/HOUSEH\_C to obtain its eigenvalues and eigen vectors.

### 3.39. Subroutine PRINT\_Ek

In this routine, the eigenvalues of the Fock matrix obtained in the subroutine BAND are written in various ASCII files. If the calculation was an RHF one, then the data is written in the file named 'bands.dat', while for the UHF calculations the up-spin eigenvalues are written in the file 'bandsUP.dat', and the down-spin ones in the file 'bandsDOWN.dat'. These files can be used for plotting the band structure using the standard graphics packages such as xmgrace(**author?**) [59] or gnuplot(**author?**) [60].

### 3.40. Subroutine DOS

This subroutine computes the density of states (DOS) and writes it in an ASCII file named 'dos.dat'. The input to the routine consists of the energy windows, and the broadening parameter (*cf.* Eq. 17).

### 3.41. Subroutine OPTICS

This is the master routine meant for evaluating the optical absorption spectrum. Several other subroutines are called in this routine to perform specific tasks. The range of frequencies over which the spectrum is to be computed, along with the line width, are read from the input file. The calculated spectrum is written in output files called 'sigma\_x.dat' for incident radiation polarized along  $x$ -axis, and 'sigma\_y.dat', for incident radiation polarized along  $y$ -axis, respectively. Furthermore, the joint-density of states is written in the file named 'jdos.dat'. The data in all these files can be visualized using packages xmgrace(**author?**) [59] or gnuplot(**author?**) [60]. In addition, several output files named 'sigma\_mn.dat', where band-specific optical absorption spectra, due to transition from the  $m^{th}$  valence band to the  $n^{th}$  conduction band, are also generated.

### 3.42. Subroutine SINCOS

This routine computes  $\cos(kR_j)$  and  $\sin(kR_j)$  for various values of  $k$  and  $R_j$ , needed for performing the Fourier transforms of various quantities.

### 3.43. Subroutine makGmat

This routine constructs the electron repulsion part of Fock matrix for the RHF calculations performed within the P-P-P model Hamiltonian.

#### 3.44. Subroutine *makGmat\_UHF*

This subroutine is analogous to the routine *makGmat*, the only difference being that it constructs the repulsion matrix separately for the up- and the down-spin electrons, and is called when UHF (as against RHF) calculations are needed.

#### 3.45. Subroutine *FOUTRA*

This subroutine performs a Fourier transforms on a given complex operator, either from the  $\mathbf{k}$ -space to the  $\mathbf{r}$ -space, or vice versa, depending upon the value of the input variable 'iflag'. Because the systems under consideration are 1D, the BZ integration is performed only in the positive part of the BZ, as the contribution of the negative part of the BZ is same as that from the positive part.

#### 3.46. Subroutine *HOUSEH\_C*

This subroutine, which originally belongs to the EISPACK library (**author?**) [58], is used for diagonalizing the Fock matrix at different  $k$  points to obtain its eigenvalues and eigenvectors. For the purpose, the Householder diagonalization approach is utilized (**author?**) [58].

#### 3.47. Subroutine *DENK\_RHF*

This subroutine constructs the density matrix in the  $k$  space, using the Bloch orbitals for the closed-shell systems, assuming that the orbitals are doubly occupied.

#### 3.48. Subroutine *DENK\_UHF*

This subroutine performs the same function for UHF calculations, which the routine *DENK\_RHF* performs for the RHF calculations. It generates different density matrices for the orbitals with  $\alpha$  and  $\beta$  spins, and also obtains the total density matrix by adding them.

#### 3.49. Subroutine *SYMMAT*

This subroutine multiplies the off-diagonal Fock matrix elements of a real-symmetric matrix by a factor of 2 to enforce the upper-triangular nature of the matrix.

#### 3.50. Subroutine *xMMEcv*

Using  $\frac{\partial F(k)}{\partial k}$  computed in the subroutine 'GRADFK', this subroutine computes the momentum matrix element  $\langle c(k)|p_x|v(k)\rangle$  defined in Eq.19 for incident radiation polarized along the  $x$ -direction.

#### 3.51. Subroutine *yMMEcv*

This subroutine computes the momentum matrix element  $\langle c(k)|p_y|v(k)\rangle$  defined in Eq.19 for the incident radiation polarized along the  $y$ -direction.



### 3.52. Function *LINESHAPE*

This function computes the Lorentzian line shape, inputs are line width, frequency of the incident radiation, and the energy difference between the conduction- and valence-band eigenvalues, at a given  $k$ -point.

### 3.53. Subroutine *SIGMA\_ABSORB*

This routine evaluates the optical absorption spectrum defined in Eq.18.

### 3.54. Subroutine *printTimeDate*

This subroutines uses the Fortran 90 intrinsic routine `DATE_AND_TIME` to print date and time.

### 3.55. Subroutine *bloch\_out*

This subroutine generates an output file named 'bloch.dat', in which the eigenvectors are written in the binary format.

## 4. Installation, input files, output files

We believe that the installation and execution of the program, as well as preparation of suitable input files is fairly straightforward. Therefore, we will not discuss these topics in detail here. Instead, we refer the reader to the README file for the details related to the installation and execution of the program. Additionally, the file 'manual.pdf' explains how to prepare a sample input file. Several sample input and output files corresponding to various example runs are also provided with this package.

## 5. Results and Discussions

In this section we demonstrate the abilities of our code by presenting results for some 1D  $\pi$ -conjugated systems such as  $t$ -PA, PPP, AGNR-11, AGNR-14, ZGNR-8 (ZGNR- $N_Z$ , denotes a ZGNR with  $N_Z$  zigzag lines across the width), and ZGNR-10. Unless otherwise specified, all the calculations are performed using the screened parameters with  $U = 8.0$  eV and  $\kappa_{i,j} = 2.0$  ( $i \neq j$ ) and  $\kappa_{i,i} = 1$ . However, later on we examine the influence of Coulomb parameters on the band structure of GNRs. In order to benchmark our code, first we use it to compute the total energy per unit cell ( $E_{cell}$ ) for  $t$ -PA and the polymer PPP, and compare it with the results obtained using our earlier P-P-P code meant for finite systems (author?) [47], with the increasing system size. We also analyze the convergence of the total energy/cell with respect to the total number of  $k$  points ( $n_k$ ) used for the BZ integration, number of cells considered for summation of exchange integral ( $n_{exc}$ , cf. Eq. 11), by means of calculations on AGNR-6. Furthermore, we present our results for the band structure, density of states, linear optical absorption spectrum of some of the systems mentioned above. The calculations and analysis of the electric field driven half-metallicity of ZGNR-14 and the electro-absorption(EA) spectrum of ZGNR-8 are also presented.

Table 1: Variation of total energy (in eV) per unit cell ( $E_{cell}$ ) of t-PA and PPP with the number of unit cells ( $N$ ) obtained using our earlier P-P-P code for finite systems(**author?**) [47], compared with the result for the infinite polymer obtained by the present code (last column).

System	$N = 5$	$N = 10$	$N = 50$	$N = 100$	Infinite Polymer (This work)
t-PA	-3.20	-3.30	-3.38	-3.39	-3.40
PPP	-11.66	-11.73	-11.79	-11.79	-11.81

### 5.1. Total energy

The variation of total energy per unit cell,  $E_{cell}$  for finite fragments of t-PA and PPP with the increasing number of cells ( $N$ ) obtained using our earlier P-P-P code for the finite systems(**author?**) [47] is tabulated in Table 1, while the  $E_{cell}$  for the same systems in the infinite polymer limit, obtained by the present code `ppp_bulk.x`, is presented in the last column of the table. The t-PA was considered in its dimerized configuration, with the single (double) bond length of 1.45Å(1.35 Å), and the corresponding hopping matrix element to be 2.232 eV (2.568 eV). In case of the polymer PPP, the intra-phenyl C-C bond length was taken to be 1.4 Å with the corresponding hopping of 2.46 eV, while the length of the single bond connecting neighboring phenyl rings was assumed to be 1.54 Å, along with the associated hopping of 2.23 eV. From table 1 it is evident that, there is excellent agreement between the two sets of calculations, which gives us confidence about the essential correctness of our code.

Next, we examine the convergence of  $E_{cell}$  for AGNR-6 with the increasing values of  $k$  points ( $n_k$ ) used for BZ integration (Fig. 1(a)) and with the increasing values of the number of unit cells in the exchange sum,  $n_{exc}$  (Fig. 1(b)). The nearest-neighbor (NN) hopping was chosen to be  $t = 2.7$  eV. From Fig. 1 it is obvious that: (a)  $E_{cell}$  converges at about  $n_k = 25$ , and remains insensitive to further increase in the value  $n_k$ , and (b)  $E_{cell}$  converges rapidly with  $n_{exc}$  and convergence is achieved for  $n_{exc} = 10$ . In both cases we have considered about 10000 cells to evaluate the Coulomb part of two electron integrals (*c.f* Eq.10). For rest of the calculations we have chosen the values :  $n_k = 50$  and  $n_{exc} = 24$ .

### 5.2. Band structure and the Density of States

Our code can also be used to perform band structure calculations, along with the associated DOS using the TB model, as well as the P-P-P model, employing both the RHF and the UHF methods. In what follows below, we present the band structure and DOS for a few of the systems, computed using our code.

#### 5.2.1. Trans-polyacetylene

The band structure of the dimerized *t*-PA obtained by the P-P-P-RHF method is presented in Fig. 2 (a), with the Fermi energy ( $E_F$ ) set to 0. The band gap occurs at  $k = \pi/a$ , and is obtained to be 2.30 eV, a value in excellent agreement with the the HOMO-LUMO gap of 2.31 eV obtained for a finite fragment of t-PA consisting of 100 unit cells, computed using our earlier molecular

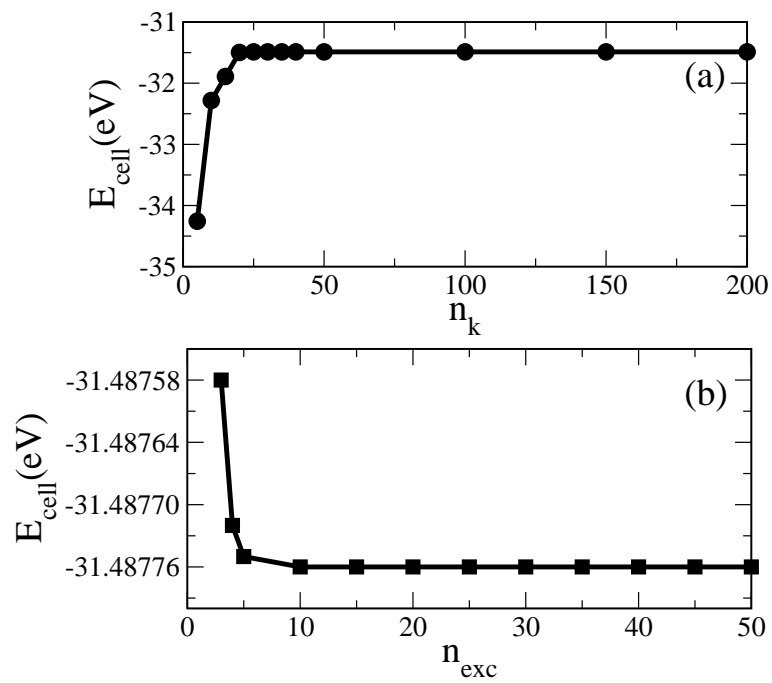


Figure 1: Variation of total energy per unit cell of AGNR-6 with respect to: (a)  $n_k$ , and (b)  $n_{\text{exc}}$ .

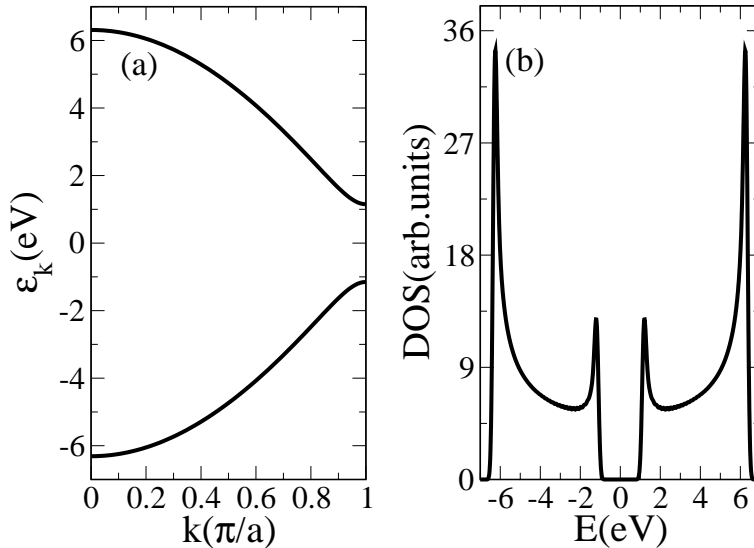


Figure 2: (a) Band structure, and (b) DOS of dimerized t-PA obtained using the P-P-P model, and the RHF method.

P-P-P code (author?) [47]. The vanishing DOS (Fig. 2(b)) around the Fermi energy characterizes the band gap, while the DOS peaks near  $E = \pm 1.15$  eV and  $E = \pm 6.3$  eV are due to the van Hove singularities at  $k = \pi/a$  and  $k = 0$ , respectively.

### 5.2.2. Graphene Nanoribbons

In this section we present the results of band structure calculations on both AGNRs and ZGNRs. Furthermore, we also examine the electricity-driven half-metallicity predicted in ZGNRs, by computing its band structure in the presence of a transverse static electric field. However, first we examine the influence of Coulomb parameters on the electronic structure of GNRs. In all the calculations on the GNRs reported in the remainder of this work, carbon-carbon nearest-neighbor distance was taken to be  $1.42 \text{ \AA}$ , and all the bond angles were assumed to be  $120^\circ$ . As far as the hopping matrix elements are concerned, for both AGNRs and the ZGNRs, the nearest-neighbor hopping was taken to be  $2.7$  eV, while, only for ZGNRs, a second nearest-neighbor hopping of  $t' = 0.27$  eV was also included.

*Influence of Coulomb parameters.* In our earlier work on GNRs (author?) [48], we proposed a set of “modified screened Coulomb parameters,” with  $U = 6.0$  eV and  $\kappa_{i,j} = 2.0$  ( $i \neq j$ ) and  $\kappa_{i,i} = 1$ , however, we did not present a detailed analysis of the parameter dependence of our results. In Tables 2 and 3 we present the results of our P-P-P-HF calculations of the band gaps of AGNRs and ZGNRs of varying widths as a function of the Coulomb parameter  $U$ , while the screening

Table 2: Band gaps of different families of AGNR- $N_A$  ( $N_A = 3p, 3p+1, 3p+2$ , ( $p \geq 1$ , is an integer) obtained using our P-P-P RHF approach for  $U = 6.0$  eV and  $U = 8.0$  eV, compared with the *ab initio* DFT and GW results of Yang *et al.*(**author?**) [13].

Width (nm)	Energy gaps (eV) for <b>3p</b> series of AGNRs			
	GW( <b>author?</b> ) [13]	DFT( <b>author?</b> ) [13]	$U = 6.0$ eV	$U = 8.0$ eV
0.61	2.72	1.13	2.31	2.65
0.98	2.01	0.68	1.39	2.01
1.35	1.68	0.55	1.17	1.63
Width (nm)	Energy gaps (eV) for <b>3p+1</b> series of AGNRs			
	GW( <b>author?</b> ) [13]	DFT( <b>author?</b> ) [13]	$U = 6.0$ eV	$U = 8.0$ eV
0.36893	5.5	2.50	3.29	3.72
0.73785	3.83	1.60	2.18	2.50
1.10678	2.83	1.13	1.64	1.90
1.47571	2.40	0.93	1.33	1.55
Width (nm)	Energy gaps (eV) for <b>3p+2</b> series of AGNRs			
	GW( <b>author?</b> ) [13]	DFT( <b>author?</b> ) [13]	$U = 6.0$ eV	$U = 8.0$ eV
0.49190	1.71	0.47	0.41	0.67
0.86083	1.18	0.33	0.31	0.50
1.22976	0.94	0.22	0.24	0.40
1.59868	0.77	0.19	0.20	0.33

defined by  $\kappa_{i,j} = 2.0$  ( $i \neq j$ ) and  $\kappa_{i,i} = 1$  is employed. Furthermore, we also compare our results to the *ab initio* DFT and GW results(**author?**) [13].

An inspection of the two tables reveals the following trends: for AGNRs, with  $U = 8.0$  eV excellent agreement is obtained between our HF band gaps and the *ab initio* GW band gaps(**author?**) [13] of the  $N_A = 3p$  family, however, for other families both with  $U = 6.0$  eV and  $U = 8.0$  eV our HF band gaps are smaller than the *ab initio* GW results but larger than the DFT results. For ZGNRs excellent agreement is obtained between our P-P-P-UHF results and the GW results(**author?**) [13] for  $U = 4.5$  eV, while with all the larger values of  $U$ , our approach overestimates the results as compared to the GW ones. Thus, we conclude that no single value of Coulomb parameter  $U$  provides good agreement between our HF results and GW results for all classes of GNRs. Therefore, in the absence of any reliable experimental data on the GNR band gaps, we have decided to use the original screened parameters of Chandross and Mazumdar(**author?**) [52], with  $U = 8.0$  eV and  $\kappa_{i,j} = 2.0$  ( $i \neq j$ ) and  $\kappa_{i,i} = 1$ .

*AGNR Band Structure.* Before we discuss the band structure of AGNRs obtained using our approach, we examine the variation of their band gaps with respect to the three aforesaid families corresponding to the widths  $N_A = 3p, 3p+1$ , and  $3p+2$ , where  $p$  ( $\geq 0$ ) is an integer. This classification is based upon the TB values of the band gaps which exhibit the relation  $E_g^{3p} \geq E_g^{3p+1} \geq E_g^{3p+2}$  ( $= 0$ )(**author?**) [10]. However, *ab initio* density-functional theory (DFT) calculations(**author?**) [10] on these ribbons predicted a different relationship  $E_g^{3p+1} \geq$

Table 3: Variation of ZGNR band gaps with the ribbon width, computed using various values of screened Coulomb parameters, and the P-P-P-UHF method, compared with the *ab initio* DFT and GW results(**author?**) [13]. Band gaps are also presented at the edge of the Brillouin Zone ( $k = \pi/a$ ), which are more or less width independent. All the gaps correspond to the spin-polarized edge states of ZGNRs.

Width (nm)	Energy gaps (eV) for ZGNRs				
	DFT( <b>author?</b> ) [13]	GW( <b>author?</b> ) [13]	$U = 4.5$ eV	$U = 6$ eV	$U = 8$ eV
1.136	0.35	1.36	1.34	1.91	3.04
1.562	0.33	1.23	1.14	1.61	2.64
1.988	0.25	1.04	1.00	1.40	2.35
2.410	0.23	0.95	0.88	1.22	2.13
Band gap (eV) at the zone boundary ( $k = \pi/a$ )					
	DFT( <b>author?</b> ) [13]	GW( <b>author?</b> ) [13]	$U = 4.5$ eV	$U = 6$ eV	$U = 8$ eV
	$\sim 0.45$	$\sim 1.95$	$\sim 1.94$	$\sim 2.84$	$\sim 4.40$

$E_g^{3p} \geq E_g^{3p+2} (\neq 0)$ , with the important result that even for  $N_A = 3p+2$ , AGNRs exhibit nonzero energy gaps, due to the fact that the bond lengths involving the edge atoms are shorter than those in the interior. When the decrease in the bond length is incorporated in the TB approach by increasing the corresponding hopping, one also obtains finite gaps for  $N_A = 3p+2$  ribbons, although the relation  $E_g^{3p} \geq E_g^{3p+1} \geq E_g^{3p+2}$  still holds. Here, we intend to investigate as to which of these relationships holds when the AGNR band gaps are computed using our P-P-P-RHF approach. In Fig. 3 we present the graph depicting the variation of the band gaps of AGNRs for all the three families, with respect to their width, computed using the screened Coulomb parameters and our P-P-P-RHF method. From the figure it is obvious that while the band gaps of  $3p$  and  $3p+1$  families are fairly close to each other for a given width, yet the relation  $E_g^{3p+1} \geq E_g^{3p} \geq E_g^{3p+2} (\neq 0)$ , in agreement with the *ab initio* DFT and GW results(**author?**) [10], is found to hold for a fairly large range of width.

Next, in Fig. 4, we present the band structure and the DOS of AGNR-14, belonging to the  $3p+2$  family, computed using our P-P-P-RHF method. It is evident from the figure that the AGNR-14 is an insulating system with a small band gap of about 0.65 eV, located at the point  $k = 0$ . The DOS presented in Fig. 4(b), naturally vanishes in the region of the gap. Furthermore, it exhibits several symmetrically placed peaks corresponding to the van Hove singularities.

*ZGNR Band Structure.* The nature of the ground state of ZGNRs is quite interesting, with several authors reporting the existence of a magnetically-ordered ground state, with oppositely oriented spins localized on the zigzag edges on the opposite sides of the ribbons(**author?**) [21, 50, 61], a result verified also in several first principles DFT calculations(**author?**) [10, 14]. As reported in our earlier work, P-P-P-UHF calculations performed using the present code also predict magnetized edge state as the ground state of ZGNRs(**author?**) [48]. Here we elaborate the underlying physics by performing TB, P-P-P-RHF and P-P-P-UHF calculations on ZGNR-10 using the present code, the results of which are

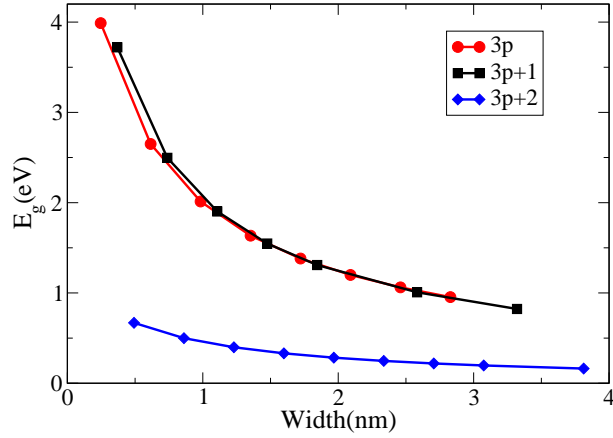


Figure 3: (Color online) Variation of the band gaps of AGNRs- $N_A$ , for  $N_A = 3p$ ,  $3p + 1$ , and  $3p + 2$ , families, with respect to their width. All calculations were performed with the original screened parameters ( $U = 8.0$  eV and  $\kappa_{i,j} = 2.0$  ( $i \neq j$ ) and  $\kappa_{i,i} = 1$ )(author?) [52] in the P-P-P model.

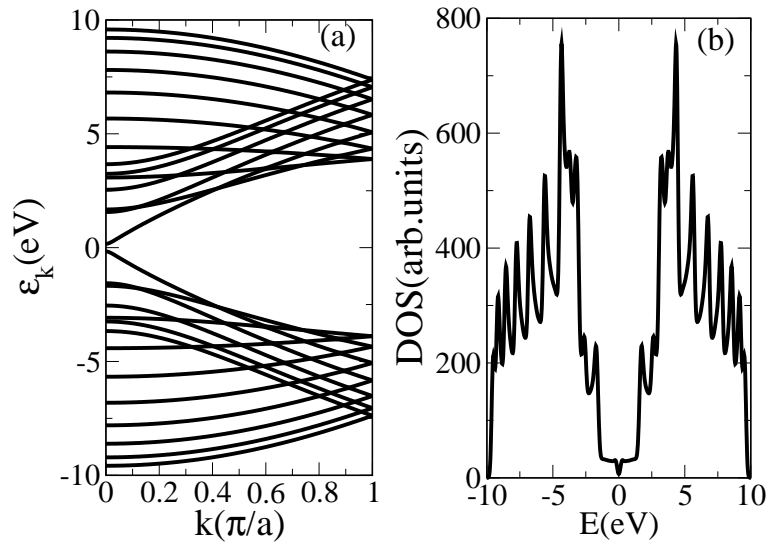


Figure 4: (a) Band structure and (b) DOS of AGNR-14 obtained by P-P-P-RHF method, obtained using the screened Coulomb parameters.

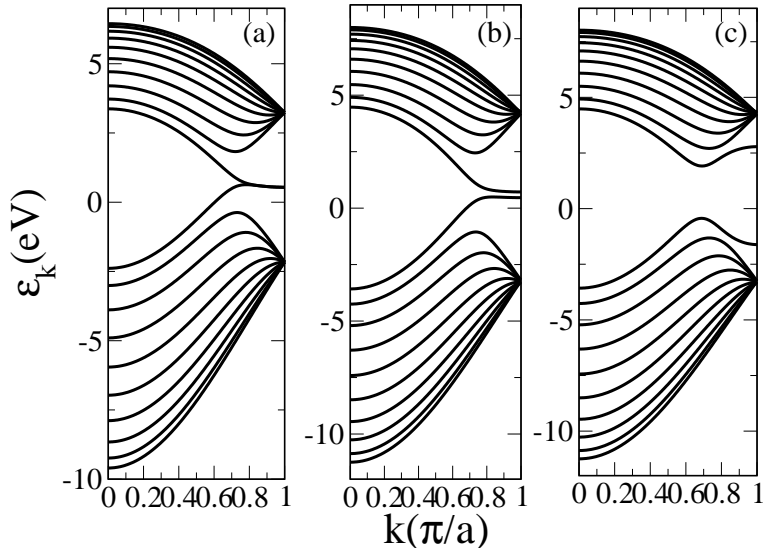


Figure 5: Band structures of ZGNR-10 obtained by: (a) TB method (b) P-P-P-RHF method, and (c) P-P-P-UHF method.

presented in Figs. 5 and 6. At the TB level ZGNR-10 (or a ZGNR of any other width) is obtained to be gapless as depicted in Fig. 5a, characterized by flat bands near  $E_F$ , leading to an intense van Hove singularity at  $E_F$  (*cf.* Fig.6a). This suggests an instability in the system, and, therefore, a possibility of a structural distortion through electron-phonon coupling, or a magnetic ordering mediated by Coulomb interactions (author?) [21]. But, the band structure of ZGNR-10 obtained by the P-P-P-RHF method (Fig.5b) is very similar to that obtained by the TB method, except for a small band gap of about 0.25 eV, which is an artifact of the RHF approach. Thus, the RHF method by its very nature predicts a non-magnetic ground state, even though it takes e-e interactions into account. However, once we perform spin-polarized calculations using the UHF approach which is based upon separate mean-fields for the up- and the down-spin electrons, we get the ground state exhibiting edge magnetism, a significant band gap of 2.35 eV (*cf.* Fig.5b), and the total energy/cell of -55.532 eV which is lower than -55.006 eV for the non-magnetic state obtained by the RHF calculations.

The fact that ground state exhibits edge magnetism is obvious from the spin-density plot for the ZGNR-10 obtained from the UHF calculations, presented in Fig. 7. As far as the numerical aspects of the UHF method are concerned, it is important to note that while performing the UHF calculations the initial guesses for solutions of the up- and down-spin Bloch orbitals must be different. Because, for ZGNRs of any width, the number of electrons of spin up- and down-spin are equal, as a result of which the UHF solutions converge to RHF results, unless the initial guess for the two spin components is different.



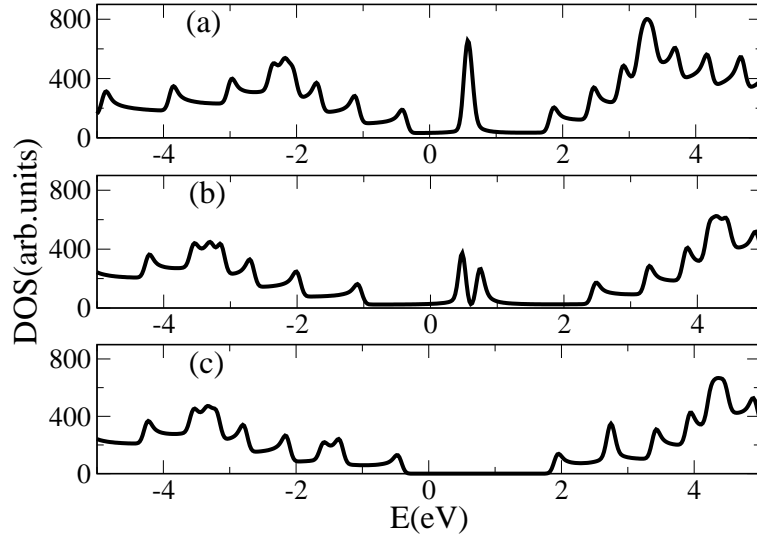


Figure 6: The density of states of ZGNR-10 obtained by: (a) tight binding method, (b) P-P-P-RHF method, and (c) P-P-P-UHF method. The Fermi energy  $E_F$  is assumed to be at  $E = 0$ .

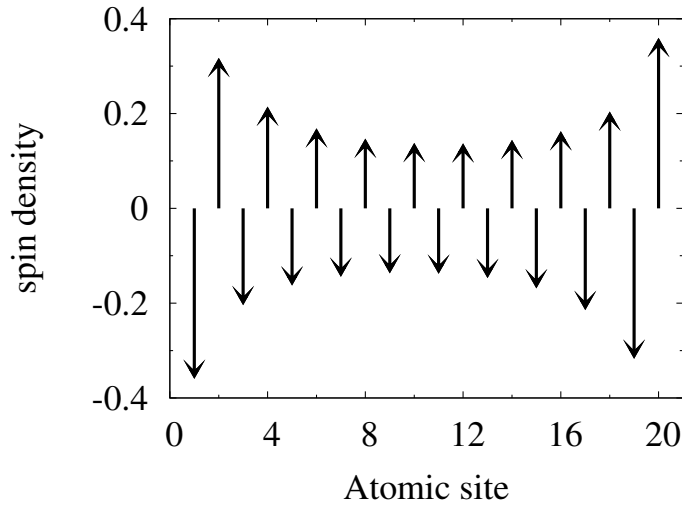


Figure 7: Spin density of ZGNR-10, obtained using the P-P-P-UHF calculations, plotted at different atomic sites of the unit cell across the width of ribbon, starting from top. Antiferromagnetic alignment of spins across the width is obvious.

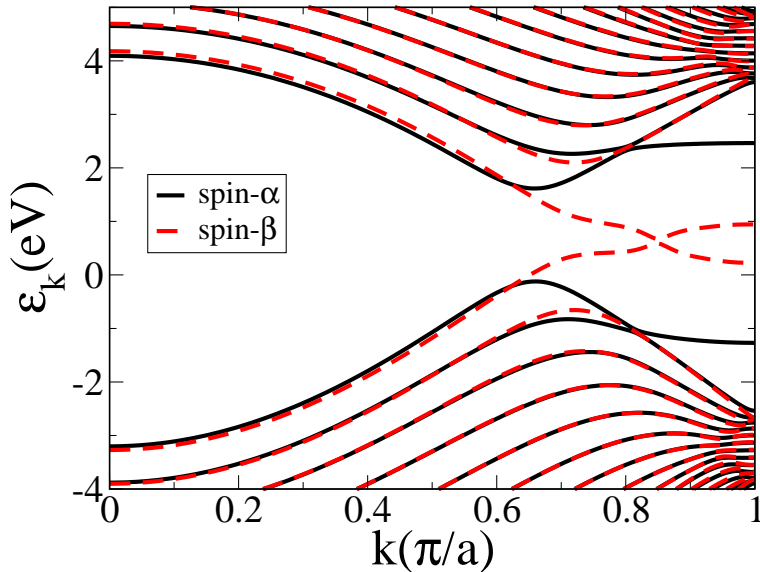


Figure 8: (Color online) Band structure of ZGNR-14 in the presence of external electric field ( $E_y = 2 \text{ V/nm}$ ), obtained by P-P-P-UHF method. The solid-black (dotted-red) lines represent the bands of  $\alpha(\beta)$ -spin electrons.

In the presence of a lateral electric field, ZGNRs exhibit half-metallic behavior (author?) [10], leading to their possible use in spintronics. In Fig. 8 we present the band structure of the ZGNR-14 exposed to a field strength of  $2 \text{ V/nm}$ . The calculations were performed using the P-P-P-UHF model with  $U = 8$ . In the absence of the field, as discussed above, the bands of the up- ( $\alpha$ ) and down-spin ( $\beta$ ) electrons are degenerate with a band gap of  $1.96 \text{ eV}$ . The degeneracy is lifted in the presence of electric field, the band gap for electrons of spin  $\alpha$  changes to  $1.74 \text{ eV}$  and the that for electrons of spin  $\beta$  changes to  $0.08 \text{ eV}$ , indicating the half-metallic nature. The band gap and the critical field strength ( $E_y^c$ ) to achieve the half-metallicity for a given ZGNR decreases with the decrease in the value of the Coulomb parameter  $U$ . For example, in case of ZGNR-14, with  $U = 4.5 \text{ eV}$ , the band gap for electrons of spin  $\beta(\alpha)$  changes to  $0.06 (0.76) \text{ eV}$ , when the ribbon is subjected to a electric field strength of  $1.0 \text{ V/nm}$ , from the gap of  $0.79 \text{ eV}$ , in the absence of the field. Furthermore, for a fixed value of  $U$ ,  $E_y^c$  decreases with increasing the width ( $w$ ) of the ZGNR, due to the decrease in the band gap and increase in the potential difference ( $V = wE_y^c$ ) between the two edges of width  $w$  (author?) [10].

### 5.3. Linear optical absorption spectrum

In our earlier work we argued that the polarization characteristics of the optical absorption in GNRs is highly dependent on the nature of its edges, and, thus, can be used to determine whether a ribbon has zigzag or armchair edges (author?) [48]. In Fig. 9 we present the optical absorption spectrum of

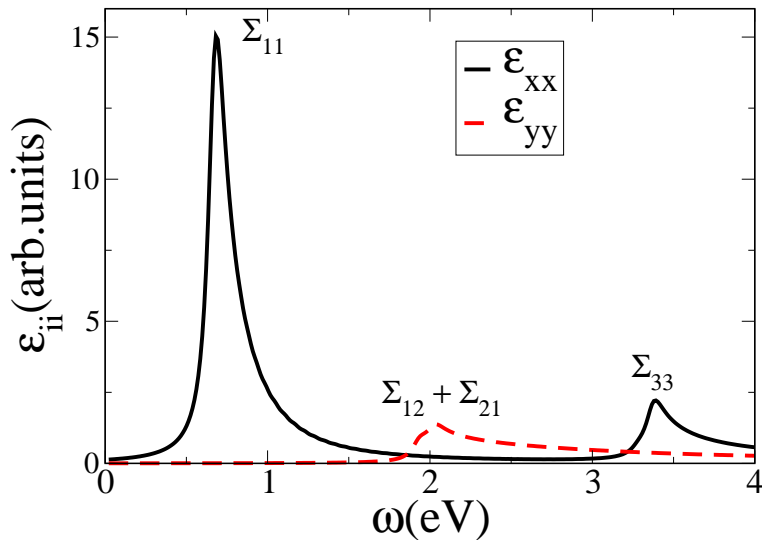


Figure 9: (Color online) Optical absorption spectrum of AGNR-14 obtained by P-P-P-RHF method. The solid-black line represents  $\epsilon_{xx}$ , while the dotted-red line represents  $\epsilon_{yy}$ . A line width of 0.05 eV was assumed.

the AGNR-14 obtained using P-P-P-RHF method. If  $\Sigma_{mn}$  denotes a peak in the spectrum due to a transition from  $m$ -th valence band (counted from top) to the  $n$ -th conduction band (counted from bottom), the peak of  $\epsilon_{xx}(\omega)$  (black line) at 0.69 eV is  $\Sigma_{11}$ , at 3.40 eV is  $\Sigma_{33}$ . The peaks of  $\epsilon_{yy}(\omega)$  (red/dotted line) at 2.05 eV correspond to  $\Sigma_{12}$  and  $\Sigma_{21}$ . The noteworthy points is that individual peaks in the spectrum correspond to either  $x$ - or  $y$ -polarized photons, consistent with the  $D_{2h}$  point group of AGNRs. Furthermore, the  $x$ - and  $y$ -polarized peaks are well separated in energy.

In Fig. 10 we present the optical absorption spectrum of ZGNR-10 obtained using the P-P-P-UHF method. The peaks in  $\epsilon_{xx}(\omega)$  are located at 2.41 eV ( $\Sigma_{11}$ ), 3.20 eV ( $\Sigma_{12}$ ), and 4.07 eV ( $\Sigma_{22}$ ), whereas the prominent peak of  $\epsilon_{yy}(\omega)$  are at 2.41 eV ( $\Sigma^{11}$ ) and 3.20 eV ( $\Sigma_{12}$ ). Therefore, in spite of the fact that the point group of ZGNRs is also  $D_{2h}$ , yet unlike AGNRs, most of the prominent peaks of ZGNR-10 exhibit mixed polarization characteristics. This is due to the fact that the edge-polarized magnetic ground state of ZGNRs no longer exhibits  $D_{2h}$  symmetry because of the fact that the reflection symmetry about the  $xz$ -plane is broken, thereby leading to mixed polarizations in the optical absorption. Thus, by performing optical absorption experiments on oriented samples of GNRs, one can predict whether a given ribbon is AGNR or ZGNR by probing the polarization characteristics of the absorption peaks.

#### 5.4. Electro-absorption spectrum

Electro-absorption (EA) spectroscopy, which consists of measuring optical absorption in the presence of a static external electric field, has been an impor-

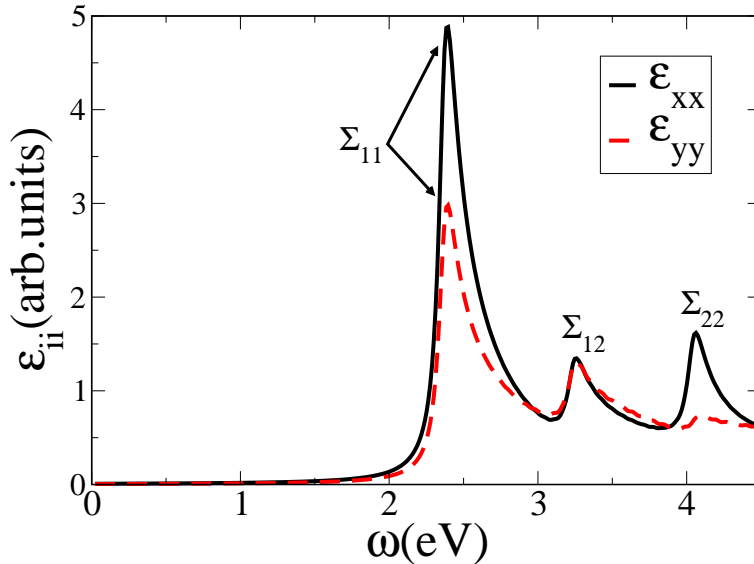


Figure 10: (Color online) Optical absorption spectrum of ZGNR-10 obtained by the P-P-P-UHF method. The solid-black line represents  $\epsilon_{xx}$ , while the dotted-red line represents  $\epsilon_{yy}$ . A line width of 0.05 eV was assumed.

tant experimental tool for probing the electronic structure and optical properties of conjugated polymers and other materials(**author?**) [62]. EA spectrum is defined as the difference of the linear absorption spectra with, and without, an external static electric field. In our earlier work we argued that the EA spectrum can be used as a probe of both the electric-field driven half-metallicity, as well as the edge magnetism of ZGNRs(**author?**) [48]. The essential physics behind it is that in the presence of a lateral external electric field, the band gap of a spin-polarized ZGNR for spin-up electrons is different from those of down spins, leading to two split optical transitions across the gap. We illustrate this in Fig. 11 which contains the EA spectrum of ZGNR-8 in the presence of a lateral external electric field of strength 1 V/nm, as well as the linear absorption without the field, for its spin-polarized ground state, computed using the P-P-P-UHF approach. The tendency towards half metallicity is apparent with the presence of two energetically split peaks corresponding to two different  $\Sigma_{11}$  transitions among up and down-spin electrons. Noteworthy point is that the two split peaks across the fundamental gaps will occur only if the ZGNR has a edge-magnetized ground state, and not when the system has a non-magnetic ground state. Therefore, if these split peaks predicted in our work can be verified in the EA spectra of the ZGNRs, it will provide an all-optical probe of determining the nature of the edges in GNRs.

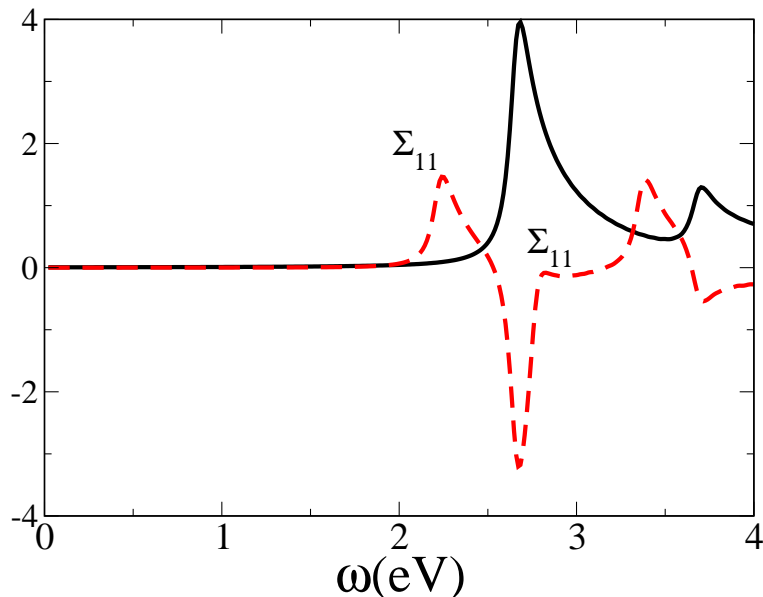


Figure 11: (Color online) Linear absorption spectrum (solid-black line), and the electro-absorption spectrum (dotted-red line) of ZGNR-8 obtained by the P-P-P-UHF method.

## 6. Conclusions and future directions

In this paper we have described our Fortran 90 program which solves the HF equations for both the closed- and open-shell 1D-periodic  $\pi$ -conjugated systems using the TB and P-P-P models. The present computer program has been written in Fortran 90 language which allows dynamic allocation of memory, thereby freeing the code from artificial limits related to array sizes. To demonstrate the capabilities of our code, we presented results of numerous test calculations on various systems including organic polymers, as well as GNRs. We presented the results of total energy calculations on the polymer t-PA and PPP, while the band structure and the density of states of t-PA and various GNRs were reported. Furthermore, we also explored the electric-field driven half metallicity of ZGNRs, as also the optical absorption spectra of both AGNRs and ZGNRs. We also reported calculations on the EA spectrum of ZGNRs, and argued that it can be used to determine the nature of edge termination in GNRs so as to differentiate between armchair and zigzag type edges.

Having developed a HF mean-field code for the 1D periodic  $\pi$ -conjugated system, our next aim is to include the electron-correlation effects for them, particularly for the band structure, as well as to account for the excitonic effects in optical absorption. Work along those directions is underway in our group, and results will be communicated in future publications.

*Acknowledgment.* We thank the Department of Science and Technology (DST), Government of India, for providing financial support for this work under Grant No. SR/S2/CMP-13/2006. K. G is grateful to Dr. S. V. G. Menon (BARC) for his continued support of this work.

## References

- [1] L. Salem, *The molecular orbital theory of conjugated systems*, W. A. Benjamin, Inc. (1966), New York.
- [2] See, e.g., D. Barieswyl, D. K. Campbell, and S. Mazumdar, in *Conjugated Conducting Polymers*, edited by H. Keiss (Springer-Verlag, Berlin, 1992), pp. 7-133.
- [3] See, e.g., L. Salem, *Molecular orbital theory of conjugated systems*, W. A. Benjamin Inc., New York (1966). W. Barford, *Electronic and Optical Properties of Conjugated Polymers* (Clarendon Press, Oxford, 2005).
- [4] D. Fichou, ed., *Handbook of Oligo- and Polythiophenes* (Wiley-VCH, Weinheim, 1999); M. A. Baldo, M. E. Thompson, and S. R. Forrest, *Nature (London)* 403 (2000) 750; S. R. Forrest, *Nature (London)* 428 (2004) 911; G. Malliaras and R. Friend, *Phys. Today* 58 (2005) 53; H. Sirringhaus, N. Tessler, and R. H. Friend, *Science* 280 (1998) 1741.
- [5] S. Novoselov, A. K. Geim, S. V. Morozov, D. Jiang, Y. Zhang, S. V. Dubonos, I. V. Grigorieva, and A. A. Firsov, *Science* 306 (2004) 666.
- [6] J. J. Palacios, J. F. Rossier, L. Brey and H. A. Fertig, *Semicond. Sci. Technology* 25 (2010) 033003.
- [7] A. K. Geim and Novoselov, *Nature Materials* 6 (2007) 183.
- [8] A. H. Castro Neto, F. Guinea, N. M. R. Peres, K. S. Novoselov, and A. K. Geim, *Rev. Mod. Phys.* 81 (2009) 109.
- [9] N. M. R. Peres, *Rev. Mod. Phys.* 82 (2010) 2673.
- [10] Y. W. Son, M. L. Cohen, and S. G. Louie, *Phys. Rev. Lett.* 97 (2006) 216803.
- [11] V. Barone, O. Hod, G. E. Scuseria, *Nano Letts.* 6 (2006) 2748.
- [12] L. Yang, M. L. Cohen, and S. G. Louie, *Nano Lett.* 7 (2007) 3112.
- [13] L. Yang, C.-H. Park, Y.-W. Son, M. L. Cohen, and S. G. Louie, *Phys. Rev. Lett.* 99 (2007) 86801.

- [14] L Yang, M. L. Cohen, and S. G. Louie, Phys. Rev. Lett. 101 (2008) 186401.
- [15] D. Prezzi, D. Varsano, A. Ruini, A. Marini, and E. Molinari, Phys. Rev. B 77 (2008) 041404.
- [16] M. Kertesz, Adv. Quant. Chem. 15 (1982) 161.
- [17] C. Pisani and R. Dovesi, Int. J. Quantum Chem. 17 (1980) 501.
- [18] A. Shukla, M. Dolg, H. Stoll and P. Fulde, Chem. Phys. Lett. 262 (1996) 213; A. Shukla, M. Dolg, P. Fulde, and H. Stoll, Phys. Rev. B. **60**, 5211 (1999).
- [19] A. Shukla, M. Dolg, and H. Stoll, Phys. Rev. B 58 (1998) 4325.
- [20] K. Nakada, M. Fujita, G. Dresselhaus, and M. S. Dresselhaus, Phys. Rev B **54**, 17954 (1996).
- [21] M. Fujita, K. Wakabayashi, K. Nakada, and K. Kusakabe, J. Phys. Soc. Jpn **65**, 1920 (1996).
- [22] M. Ezawa, Phys. Rev. B **73**, 045432 (2006).
- [23] J. Fernández-Rossier and J. J. Palacios, Phys. Rev. Lett. **99**, 177204 (2007).
- [24] O. V. Yazyev, Phys. Rev. Lett. **101**, 037203 (2008).
- [25] J. Jung and A. H. MacDonald, Phys. Rev. B **79**, 235433 (2009).
- [26] A. Yamashiro, Y. Shimoi, K. Harigaya, and K. Wakabayashi, Phys. Rev. B **68**, 193410 (2003).
- [27] R. Pariser and R. G. Parr, J. Chem. Phys. **21**, 767 (1953); J. A. Pople, Trans Faraday Soc. **49**, 1275 (1953).
- [28] A. Shukla and S. Mazumdar, Phys. Rev. Lett 83 (1999) 3944.
- [29] H. Ghosh, A. Shukla, and S. Mazumdar, Phys. Rev. B 62 (2000) 12763.
- [30] A. Shukla, H. Ghosh, and S. Mazumdar, Synth. Met. 116 (2001) 87.
- [31] A. Shukla, Phys. Rev. B 65 (2002) 125204.
- [32] A. Shukla, H. Ghosh, and S. Mazumdar, Phys. Rev. B 67 (2003) 245203.
- [33] A. Shukla, H. Ghosh, and S. Mazumdar, Synth. Met. 141 (2004) 59.

- [34] A. Shukla, Chem. Phys. 300 (2004) 177.
- [35] A. Shukla, Phys. Rev. B 69 (2004) 165218.
- [36] P. Sony and A. Shukla, Phys. Rev. B 71 (2005) 165204.
- [37] A. Shukla and P. Sony, Synth. Met. 155 (2005) 368.
- [38] P. Sony and A. Shukla, Synth. Met. 155 (2005) 316.
- [39] P. Sony and A. Shukla, Phys. Rev. B 75 (2007) 155208.
- [40] P. Sony and A. Shukla, J. Chem. Phys. 131 (2009) 014302.
- [41] See, *e.g.*, K. Jug, Int. J. Quant. Chem. 37 (1990) 403.
- [42] Z. G. Soos, S. Ramasesha, and D. S. Galvão, Phys. Rev. Lett. 71 (1993) 1609.
- [43] A. Ye, Z. Shuai, and J. L. Brédas, Phys. Rev. B 65 (2002) 045208.
- [44] C. Raghu, Y. Anusooya Pati, and S. Ramasesha, Phys. Rev. B 66 (2002) 035116.
- [45] R. J. Bursill and W. Barford, J. Chem. Phys. 130 (2009) 234302.
- [46] D. Psiachos and S. Mazumdar, Phys. Rev. B 79 (2009) 155106.
- [47] P. Sony and A. Shukla, Comp. Phys. Comm. 181 (2010) 821.
- [48] K. Gundra and A. Shukla, Phys. Rev B 83 (2011) 075413.
- [49] K. Gundra and A. Shukla, Phys. Rev. B 84 (2011) 075442 .
- [50] K. Nakada, M. Igami , K. Wakabayashi, and M. Fujita, Mol. Cryst. Liq. Cryst. 310 (1998) 225.
- [51] K. Ohno, Theor. Chim. Acta 2 (1964) 219.
- [52] M. Chandross and S. Mazumdar, Phys. Rev. B 55 (1997) 1497.
- [53] A. Szabo and N. S. Ostlund, Modern quantum chemistry (Dover publications, Inc, 1996).
- [54] J. M. André, D. P. Vercauteren, V. P. Bodart, J. G. Fripiat, J. Comp. Chem. 5 (1984) 535.
- [55] T. G. Pedersen, K. Pedersen, and T. B. Kriestensen, Phys. Rev. B 63 (2001) 201101(R).
- [56] W. H. Press, F. A. Teukolsky, W. T. Vetterling and B. P. Flannery, *Numerical Recipes Example Book (Fortran)*, Cambridge University Press (1992).



- [57] A. Kokalj, *Comp. Mat. Sci.* 28 (2003) 155.
- [58] B. Smith, J. Boyle, J. Dongarra, B. Garbow, Y. Ikebe, V. Klema, and C. Moler, *Matrix Eigenvalues Routines, EISPACK Guide, Lecture Notes in Computer Science*, Vol. 6, Springer Verlag (1976).
- [59] Xmgrace is a two-dimensional plotting tool for X Window based systems available at URL <http://plasma-gate.weizmann.ac.il/Grace>.
- [60] Gnuplot is a public domain command-line driven interactive data and function plotting utility available at URL <http://www.gnuplot.info>.
- [61] S. Okada and A. Oshiyama, *Phys. Rev. Lett.* **87**, 146803 (2001).
- [62] See, *e.g.*, M. Liess, S. Jeglinski, Z. V. Vardeny, M. Ozaki, K. Yoshino, Y. Ding, and T. Barton, *Phys. Rev. B* 56 (1997) 15712.